Title

A double-difference method for high-resolution acoustic tracking using a deep-water vertical array

Journal

The Journal of the Acoustical Society of America, 142(6)

ISSN

0001-4966

Authors

Tenorio-HallÃ©, Ludovic
Thode, Aaron M
Sarkar, Jit
et al.

Publication Date

2017-12-01

DOI

10.1121/1.5014050

Data Availability

The data associated with this publication are available upon request.

Peer reviewed

A double-difference method for high-resolution acoustic tracking using a deep-water vertical array

Ludovic Tenorio-Hallé, Aaron M. Thode, Jit Sarkar, et al.

Citation: The Journal of the Acoustical Society of America **142**, 3474 (2017); doi: 10.1121/1.5014050
View online: https://doi.org/10.1121/1.5014050
View Table of Contents: https://asa.scitation.org/toc/jas/142/6
Published by the Acoustical Society of America

A double-difference method for high-resolution acoustic tracking using a deep-water vertical array

Ludovic Tenorio-Hallé,[a] Aaron M. Thode, Jit Sarkar, Christopher Verlinden, Jeffrey Tippmann, William S. Hodgkiss, and William A. Kuperman
Marine Physical Laboratory, Scripps Institution of Oceanography, University of California San Diego, La Jolla, California 92093-0238, USA

(Received 23 February 2017; revised 3 November 2017; accepted 8 November 2017; published online 8 December 2017)

Ray-tracing is typically used to estimate the depth and range of an acoustic source in refractive deep-water environments by exploiting multipath information on a vertical array. However, mismatched array inclination and uncertain environmental features can produce imprecise trajectories when ray-tracing sequences of individual acoustic events. "Double-difference" methods have previously been developed to determine fine-scale relative locations of earthquakes along a fault [Waldhauser and Ellsworth (2000). Bull. Seismolog. Soc. Am. **90**, 1353–1368]. This technique translates differences in travel times between nearby seismic events, recorded at multiple widely separated stations, into precise relative displacements. Here, this method for acoustic multipath measurements on a single vertical array of hydrophones is reformulated. Changes over time in both the elevation angles and the relative arrival times of the multipath are converted into relative changes in source position. This approach is tested on data recorded on a 128-element vertical array deployed in 4 km deep water. The trajectory of a controlled towed acoustic source was accurately reproduced to within a few meters at nearly 50 km range. The positional errors of the double-difference approach for both the towed source and an opportunistically detected sperm whale are an order of magnitude lower than those produced from ray-tracing individual events.
 https://doi.org/10.1121/1.5014050

[JAC] Pages: 3474–3485

I. INTRODUCTION

Passive acoustic monitoring offers a non-invasive approach for localizing and tracking acoustic sources such as marine mammals, and has numerous academic, industrial, and naval applications. A standard approach for localizing impulsive signals is to measure the difference in detected arrival times of a signal across multiple hydrophones, assuming a spatially homogenous sound speed and conducting hyperbolic localization (Watkins and Schevill, 1972). However, the separation between the sensors generally needs to be at least 20% of a source's range for this technique to work. Thus, in order to locate a source over any significant region, multiple hydrophone stations need to be deployed across at least several kilometers range to create the required aperture.

More recently, methods for long-range tracking of marine mammals in deep water using a short aperture array of hydrophones have been developed (Tiemann *et al.*, 2006; Mathias *et al.*, 2013). The term "short" refers to the aperture of the array relative to the water depth, not relative to an acoustic wavelength, and the term "deep water" refers to water depths that greatly exceed the acoustic wavelength of the lowest frequency component in a signal.

These tracking techniques are mostly based on ray theory, exploiting the multipath arrival information [elevation angle and relative time of arrival (RTOA)] present in a signal's refracted and reflected ray arrivals across the array aperture. By modeling the back-propagation, or "ray-tracing," detected ray arrivals into the waveguide, the source's location can be determined by measuring where the rays converge (Fig. 1). This method has been defined as either ray-tracing or matched-field processing (MFP; Fizell and Wales, 1985), the latter term covering situations where RTOA information has been incorporated into the ray-propagation model. Sperm whales have been the focus of several of these tracking studies because of the nature of their vocalizations, which can be characterized as a series of loud and impulsive broadband clicks (Goold and Jones, 1995), which are convenient for multipath detection (Thode *et al.*, 2002; Zimmer *et al.*, 2003; Thode, 2004).

While ray-tracing methods allow localizing at long ranges relative to the array aperture, they often yield significant uncertainties in the position of the source due to several factors. Because of the lack of extensive field measurements, environmental propagation models are typically assumed to be range independent, even though the underlying environment varies with range. The resulting mismatch in the modeled sound speed profile can therefore be an important source of error when applying ray-tracing, especially at longer ranges. Another potential source of error is the array inclination, or tilt, which affects the measured elevation angles of rays. Because of these errors, tracking a moving source by individually ray-tracing a series of acoustic events often yields a trajectory with large error estimates.

Various adaptive filtering and state-state techniques like Kalman filtering can be adapted for smoothing acoustic

[a]Electronic mail: ltenorio@ucsd.edu

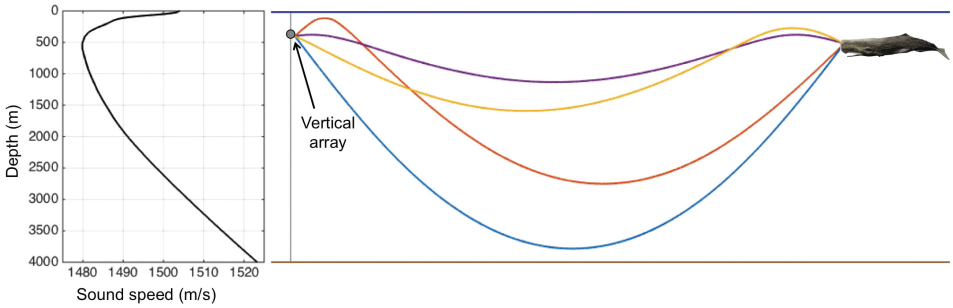

FIG. 1. (Color online) Illustration of two-dimensional (2D) ray-tracing using a vertical array. Rays detected at the array are back-propagated into the waveguide, whose sound speed profile is known (left of the image), in order to determine the depth and range of the vocalizing sperm whale (right of the image).

trajectories, essentially by incorporating information from previous localizations into the next estimate. However, this approach requires making assumptions about the behavior of the system, such as speed and heading, for example (Evensen, 2009). Here, we are interested in techniques that rely entirely on measured data and not on interpolative or smoothing approaches.

Methods for high-resolution relative localization of earthquakes are common in seismology whenever seismic events in close spatial proximity are detected at multiple sensors (Poupinet *et al.*, 1984; Ito, 1985; Fremont and Malone, 1987; Shearer, 1997). These methods are based on measuring the differences in travel times between sets of events to determine the relative location of these events. A popular and efficient formulation of this approach is the "double-difference" method by Waldhauser and Ellsworth (2000), which will be subsequently labeled as "WE." The technique minimizes the residuals between measured and modeled travel times for clusters of nearby earthquakes recorded across common stations. This approach assumes the propagation paths of sets of nearby earthquakes are similar enough that they share the same systematic errors in the modeled travel times caused by environmental perturbations and/or instrument timing error. The double-difference method has been adapted for tracking fin whales in the northeast Pacific using a network of seafloor seismic stations (Wilcock, 2012), but to our knowledge has not been previously applied to multipath tracking from a single array deployment.

This paper presents how double-difference methods can be adapted to a deep water waveguide to track a moving acoustic source at long ranges, using multipath on a single vertical hydrophone array, instead of separate direct arrivals on a seismic network of widely spaced recorders. This approach, which usually requires relatively high signal-to-noise ratio (SNR) signals, is shown to yield much higher precision than standard ray-tracing results, and can reduce systematic errors arising from environmental mismatch and array tilt uncertainties. The method is tested on a towed acoustic source whose position is independently measured throughout its deployment. Results from applying this technique to opportunistically measured sperm whales are also presented and discussed.

II. THEORY

A. Nomenclature

Consider a two-dimensional waveguide (a vertical range/depth slice of the ocean) in which multiple acoustic events from a moving source are received on a vertical array of hydrophones. Figure 2 schematically illustrates two acoustic ray paths α and β reaching the vertical array, each propagating from two time-separated events i and j. In theory, the events need not be generated by the same source, but must be sufficiently spatially and temporally close to each other such that the difference in propagation environments between two events is nearly homogenous, and that at least two ray paths from each event traverse similar propagation paths to the receiver. If T^i_α represents the travel time along a particular ray path α from a given acoustic event i to the array, then the RTOA between two ray paths α and β is defined here as

$$\Delta T^i_{\alpha\beta} = T^i_\alpha - T^i_\beta, \tag{1}$$

and the difference between the RTOAs of the two events i and j becomes

$$\Delta T^{ij}_{\alpha\beta} = (T^i_\alpha - T^i_\beta) - (T^j_\alpha - T^j_\beta). \tag{2}$$

Note that Eq. (2) effectively removes the effects of range-dependent sound speed fluctuations between the array and the two events, because the time perturbations generated by these fluctuations affect both events and are thus subtracted out in Eq. (2). Let the "elevation angle" of a ray across the vertical array be defined as the arrival angle measured relative to the horizontal with positive angles pointing toward the seafloor and negative angles pointing toward the surface. The elevation

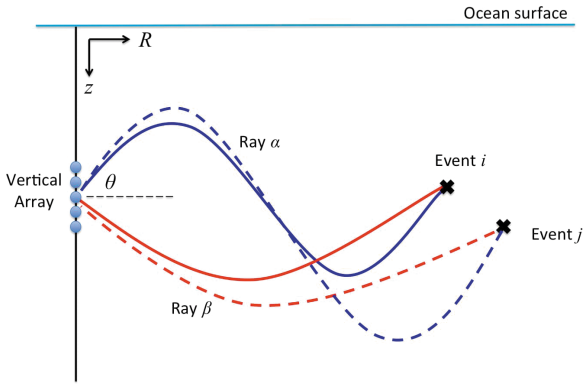

FIG. 2. (Color online) Schematic diagram of two nearby acoustic events i and j, each producing two acoustic rays α and β. A given ray path follows a slightly different trajectory from one event to the other and, therefore, arrives at the vertical array with slightly different elevation angles and RTOA for each event. However both experience the same range-dependent fluctuations in sound speed between the events and the vertical array.

angle of ray path α from an acoustic event i is then noted θ^i_α. Following the same logic as for the ray travel times, Eq. (2) can be rewritten in terms of the relative differences in elevation angles (RDEAs) between rays α and β and events i and j,

$$\Delta\theta^{ij}_{\alpha\beta} = (\theta^i_\alpha - \theta^i_\beta) - (\theta^j_\alpha - \theta^j_\beta). \tag{3}$$

Note that Eq. (3) removes any measurement bias arising from incorrect estimates of array inclination, assuming no changes in array inclination occur between events i and j.

B. Double-difference equations for a vertical array

The double-difference method minimizes residuals between *differences* in measured and modeled travel times for clusters of nearby events recorded on the same sets of sensors (WE). The technique assumes that the quantities in Eqs. (2) and (3) remove or reduce systematic errors in modeling or recording. Differences in relative travel times between event pairs are then translated into positional changes, permitting high-resolution relative localizations of the events. The original double-difference equations in WE can be rewritten in terms of the RTOA [Eq. (2)] and RDEA [Eq. (3)] instead of the absolute travel times. For a pair of events i and j, whose ray paths α and β are detected on a vertical array of sensors, the resulting "double difference" equations are as follows:

$$\frac{\partial \Delta T^i_{\alpha\beta}}{\partial R}\Delta R^i + \frac{\partial \Delta T^i_{\alpha\beta}}{\partial z}\Delta z^i - \frac{\partial \Delta T^j_{\alpha\beta}}{\partial R}\Delta R^j - \frac{\partial \Delta T^j_{\alpha\beta}}{\partial z}\Delta z^j = \left(\Delta T^{ij}_{\alpha\beta}\right)^{\text{meas}} - \left(\Delta T^{ij}_{\alpha\beta}\right)^{\text{mod}}, \tag{4}$$

$$\frac{\partial \Delta\theta^i_{\alpha\beta}}{\partial R}\Delta R^i + \frac{\partial \Delta\theta^i_{\alpha\beta}}{\partial z}\Delta z^i - \frac{\partial \Delta\theta^j_{\alpha\beta}}{\partial R}\Delta R^j - \frac{\partial \Delta\theta^j_{\alpha\beta}}{\partial z}\Delta z^j = \left(\Delta\theta^{ij}_{\alpha\beta}\right)^{\text{meas}} - \left(\Delta\theta^{ij}_{\alpha\beta}\right)^{\text{mod}}, \tag{5}$$

where $(\,)^{\text{meas}}$ and $(\,)^{\text{mod}}$ denote the measured and modeled RTOAs and RDEAs, respectively, in Eqs. (2) and (3), and $(\Delta R^i, \Delta z^i)$ and $(\Delta R^j, \Delta z^j)$ represent the range and depth adjustments required for events i and j in order for the model to better fit the data. For N events with a total of M measurements (both RTOA and RDEA), Eqs. (4) and (5) can be compactly expressed in matrix form as

$$\mathbf{Gm} = \mathbf{d} \tag{6}$$

where $\mathbf{G}$ is a $M \times 2N$ matrix of partial derivatives, $\mathbf{m}$ is a $2N$ vector of positional adjustments, and $\mathbf{d}$ is the set of M residuals on the right-hand sides of Eqs. (4) and (5). Note that Eqs. (2)–(5) differ slightly from those presented in WE. The equations presented here use α and β to represent acoustic ray paths, instead of individually placed seismic stations. Furthermore, the residuals on the right-hand sides of Eqs. (4) and (5), defined as "double-differences" in the original paper, have technically become "triple-differences" here, as they represent *differences* between measurements and models of *differences* between two events of RTOAs or RDEAs (which are themselves *differences* of arrival times or angles between two ray paths). A consequence of this reformulation is that the absolute times at which events i and j are generated, which were additional unknown variables in the original expressions, have been eliminated.

For a given event pair i and j, Eqs. (4) and (5) are first solved using estimates of the absolute event locations as an initial model, which can be provided by initial ray-tracing of one of the events. Figure 3(a) shows how the resulting components of $\mathbf{m}$ are then used to readjust event positions. This process is then re-iterated using the updated modeled positions of each event, until the residuals on the right-hand sides of Eqs. (4) and (5) are minimized. The final value of the residuals provides an estimate of the localization errors for the events, as will be discussed in Sec. II C.

The partial derivatives (or "ray derivatives") in these equations are calculated for the current modeled position of the source. From basic ray theory, it can be shown that

$$\frac{dT}{dR} = \frac{1}{c(z)}\cos(\theta)(z) \equiv p, \tag{7}$$

$$\frac{dT}{dz} = \frac{1}{c(z_s)}\sin(\theta)(z_s) \equiv \eta(z_s), \tag{8}$$

where $c(z)$ is the depth-dependent sound speed and z_s denotes the depth of the source. p is known as the ray parameter, or horizontal slowness, which is constant along a given ray path in a range-independent propagation environment, and $\eta(z)$ is known as the vertical slowness on the medium (Cornuelle, 1985; Frisk, 1994; Shearer, 1999).

C. Double-difference equations for a homogeneous environment

It is possible for an environment to be range dependent over long distances (e.g., on the order of tens of kilometers

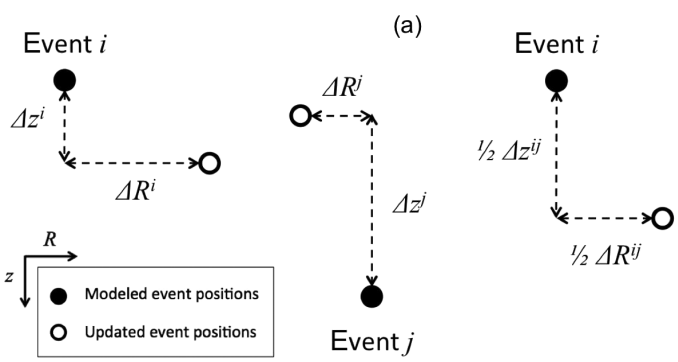

FIG. 3. Schematic diagram demonstrating the repositioning of events using the double-difference: (a) using Eqs. (4) and (5) and (b) assuming a homogenous environment using Eqs. (9) and (10).

between an event cluster and receiver), but still be treated as effectively homogenous over the region connecting two consecutive events (e.g., tens of meters for consecutive events detected from a moving source). Further simplifications in Eqs. (4) and (5) can be then made by assuming that the sound speed gradients are effectively identical inside the spatial region containing events i and j. Equations (4) and (5) then reduce to

$$\frac{\partial \Delta T^{ij}_{\alpha\beta}}{\partial R}\Delta R^{ij} + \frac{\partial \Delta T^{ij}_{\alpha\beta}}{\partial z}\Delta z^{ij} = \left(\Delta T^{ij}_{\alpha\beta}\right)^{\text{meas}} - \left(\Delta T^{ij}_{\alpha\beta}\right)^{\text{mod}}, \tag{9}$$

$$\frac{\partial \Delta \theta^{ij}_{\alpha\beta}}{\partial R}\Delta R^{ij} + \frac{\partial \Delta \theta^{ij}_{\alpha\beta}}{\partial z}\Delta z^{ij} = \left(\Delta \theta^{ij}_{\alpha\beta}\right)^{\text{meas}} - \left(\Delta \theta^{ij}_{\alpha\beta}\right)^{\text{mod}}, \tag{10}$$

where the derivatives above are the average of the derivatives evaluated at the locations of events i and j. Note that Eqs. (10) and (11) now solve for ΔR^{ij} and Δz^{ij}, the adjustments in range and depth separation between events i and j [Fig. 3(b)], instead of ΔR^{i}, Δz^{i}, ΔR^{j}, and Δz^{j}, which adjust the range and depth of each event individually, as seen in Fig. 3(a). This simplification reduces the number of variables in Eq. (6) from $2N$ to $2(N-1)$ and provides an option for Eqs. (9) and (10) to be solved independently from other event pairs. The movements of a source can therefore be estimated one event pair at a time, instead of having to solve for the relative position of each event in the entire track all at once, as would be the case for the full "inhomogeneous" problem.

For each pair of events there are two equations [Eqs. (9) and (10)] and two unknowns (ΔR^{ij} and Δz^{ij}), so a minimum of two shared ray paths between the model and the measurements is required for every iteration. If this requirement is not met, the system becomes under-determined and the separation between the pair of events cannot be determined. This method therefore requires that pairs of events occur close enough together in space for them to share similar ray paths.

It is possible for the model and the measurements of an event pair to share more than two ray paths in common. In this case, the system becomes over-determined, which gives an option to solve the system using only Eq. (9), ignoring the RDEA elevation angle measurements. This approach is defined here as the "RTOA-only" double-difference, as opposed to the "full" double-difference approach that uses the RDEA measurements. Unless otherwise specified, subsequent use of the term double-difference method below refers to the full reformulated double-difference.

D. Error estimates for double-difference computations

Error estimates for double-difference computations can be computed using bootstrap or jackknife resampling of residual values, or singular-value decomposition (SVD; WE). The small numbers of events used in this paper makes the use of the SVD approach straightforward and practical (Press, 1992). The $M \times 2(N-1)$ matrix $\mathbf{G}$ defined in Eq. (6) has a SVD of $\boldsymbol{G} = \boldsymbol{U}\boldsymbol{\Lambda}\boldsymbol{V}^T$, where $\boldsymbol{\Lambda}$ is a diagonal matrix of singular values, $\mathbf{U}$ is an $M \times M$ matrix with orthogonal columns, and $\mathbf{V}$ is a $2(N-1) \times 2(N-1)$ matrix with orthogonal columns.

Mimicking the notation of WE, the error estimate σ_i of the ith component of the vector $\mathbf{m}$ in Eq. (6) becomes

$$\sigma_i = \sqrt{C_{ii} \cdot \sigma_d^2}, \tag{11}$$

where C_{ii} is the ith diagonal element of the covariance matrix $\boldsymbol{C} = \boldsymbol{V}\boldsymbol{\Lambda}^{-2}\boldsymbol{V}^T$, and σ_d^2 is the variance of the final residuals [elements of $\mathbf{d}$ in Eq. (6)]

$$\sigma_d^2 = \frac{\sum_{k=1}^{2(N-1)} (d_k - \bar{\boldsymbol{d}})^2}{2N-3}, \tag{12}$$

where $\bar{\boldsymbol{d}}$ is the mean of $\mathbf{d}$ (WE).

In the full case where both RTOA and RDEA measurements are made (and thus the components of $\mathbf{d}$ have different units), Eq. (12) is computed independently for the RTOA and RDEA residuals, and then each row of $\mathbf{G}$ is rendered unitless by dividing it by the appropriate value of $\sigma_{d,\text{RTOA}}$ or $\sigma_{d,\text{RDEA}}$. The SVD is performed, and Eq. (11) then reduces to $\sigma_i = \sqrt{C_{ii}}$.

III. METHODS

A. Equipment

Acoustic data were collected on the mid-frequency noise array (MFNA), which was designed and built by the Marine Physical Laboratory (MPL) at the Scripps Institution of Oceanography (see supplementary material[1]). This drifting vertical array consists of 128 elements with 0.1 m spacing (7.5 kHz half wavelength), creating an aperture of 12.7 m. Vertical inclinometers were attached on the top and bottom elements of the assembly to monitor the array tilt. Data from each channel were sampled at 25 kHz and stored autonomously with 16-bit resolution. The system also had the capability of transmitting data via an 802.11 wireless connection close to a monitoring vessel.

An ITC-2040X acoustic source built by International Transducer Corporation (ITC, Santa Barbara, CA) was used as a sound source during the experiment. It was programmed to produce one second long, frequency-modulated (FM) linear sweeps from 3 to 9 kHz at 140 dB re 1 μPa at 1 m, which were repeated every second. A depth sensor attached to the source recorded the depth of the tow to within 1-m resolution once every 30 s.

B. Experiment

The MFNA was deployed at 330 m depth off the coast of San Diego, CA, in a region of flat bathymetry 4 km deep. The deployment occurred at 22:00 UTC on February 17, 2014 at 31.72° N and 122.12° W and was recovered at 14:00 UTC on February 19 at 31.7° N and 122.01° W, corresponding to a drift of ~10 km. The inclinometer data on February 18 showed that the tilt at top of the array stayed fairly constant, just below 1 degree, whereas at the lower end of the array, the tilt showed slow fluctuations between 1 and 2 degrees throughout the day, suggesting a slight catenary.

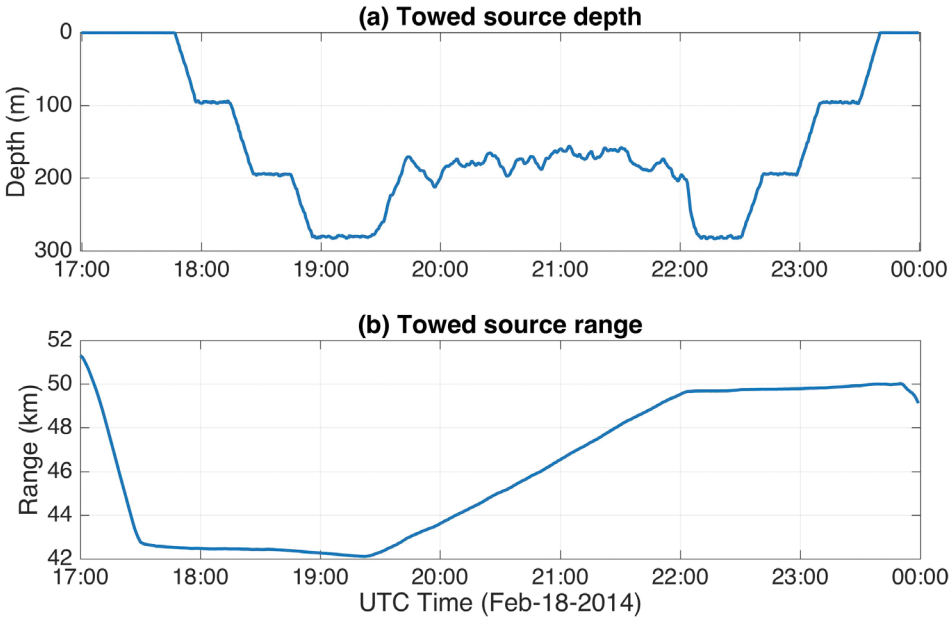

FIG. 4. (Color online) Depth (a) and range (b) trajectories of the towed acoustic source from the MFNA array during its deployment from 17:00 UTC on February 18, 2014 to 0:00 UTC on February 19, 2014.

Figure 4 shows the measured depth and range of the towed acoustic source with respect to the array, throughout the deployment. The source was deployed at 32.12° N and 122.18° W, around 17:00 UTC on February 18, from R/V Melville. Between 17:00 and 19:00 UTC, it was lowered to almost 300 m depth, with pauses every 100 m. The source was then towed away from the array at a depth slightly less than 200 m, over about 7 km, from 20:00 to 22:00 UTC. After that, the source was lowered to almost 300 m depth and then brought back up to the surface, once again pausing every 100 m, until it was recovered shortly before 0:00 UTC on February 19, at 32.17° N and 122.2° W. The drift of the array during the entire deployment of the acoustic source was about 1.5 km. The horizontal range between the source and the array was assumed to be the distance between the array and the vessel. Since the source is being towed ∼200 m behind the vessel, this assumption would yield an absolute offset between −200 m and +200 m from the true position, depending on the vessel's heading. However, the inclination of the towed array cable remained steady throughout the tow, indicating that the relative range separations between towed array positions was the same as the relative range shift of the ship measured via the Global Positioning System (GPS).

In addition to the FM sweeps broadcasted from the towed source, sperm whale clicks were opportunistically recorded over the same time period in the data collected on the vertical array. Occasional humpback whale and dolphin signals were also encountered.

C. Sound speed profile

Figure 5(a) shows the sound speed profile used in this analysis. Over the course of the experiment 15 CTD (conductivity temperature–depth) measurements were conducted to a depth of 2 km, from which an average sound speed profile was derived for the upper portion of the water column. These measured data are consistent with historical data for this region in February (Locarnini *et al.*, 2013) and shows a minimum sound speed close to 500 m depth. The lower portion of the profile down to the seafloor was then extrapolated based on historical models. A decaying exponential function was used to smoothly transition from the measured profile to the extrapolated linear function.

D. Data processing: Measuring elevation angle and RTOA of rays

In order to identify and measure the RTOA and RDEA of individual ray arrivals, acoustic events (towed source signals or sperm whale clicks) are plotted as two-dimensional (2D) migration plots, which display arrival angle versus time. These

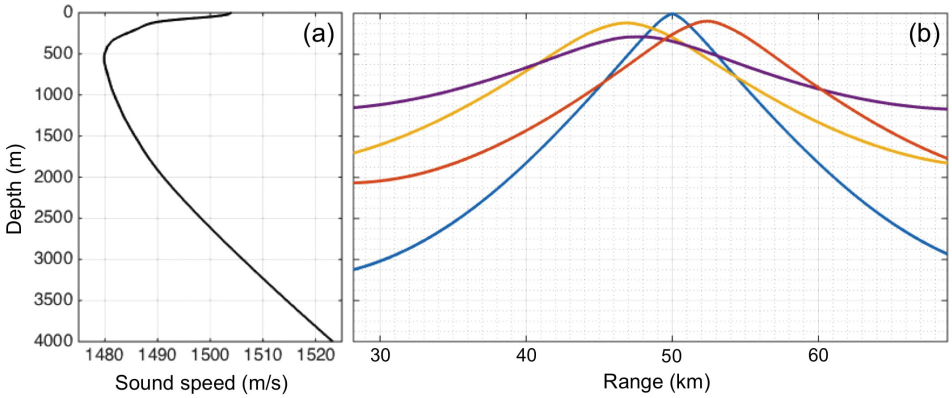

FIG. 5. (Color online) Example of propagation modeling. (a) Sound speed profile used in this analysis. The top 2000 m are based on averaged conductivity–temperature–depth (CTD) measurements conducted during the experiment. The lower portion of the profile down to the seafloor at 4000 m was extrapolated. (b) Example of simple ray-trace propagation modeling of a towed source event. Appendix B details how the best-fit position is estimated from ray paths that do not converge at a single point.

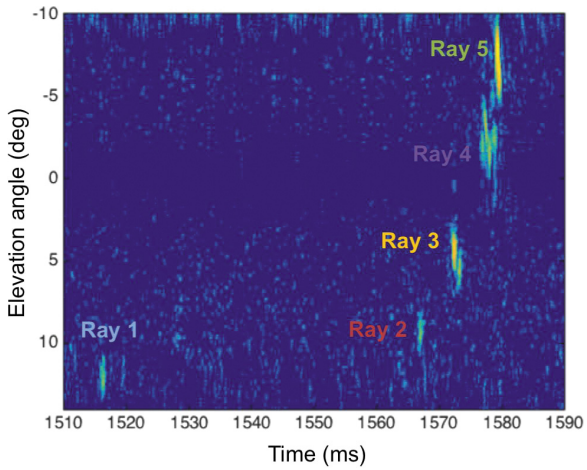

FIG. 6. (Color online) Migration plot of a matched filtered FM sweep signal from the towed source at 22:36 UTC on February 2014. Five main rays, arriving at distinct times and elevation angles, can be identified.

plots are computed by applying time-delay and sum beamforming to the data with an angular resolution of 0.1 degrees.

For the towed source, the FM nature of the signals it produces makes individual rays difficult to identify and RTOA measurements inaccurate if the migration plot is produced directly from the raw signal. Because the characteristics of these signals are known precisely, matched filtering was used to increase the SNR and yield more precise measurements (Skolnik, 1962). This process converts the FM signals from the source into single impulses, allowing RTOAs between rays to be measured more precisely. Figure 6 shows an example of a migration plot from a matched filtered towed source signal. Note that for sperm whale clicks, it was not necessary to apply a matched filter as their signals are already broadband impulses.

The arrival times and angles for each ray path were measured by taking the local maxima of a manually selected region on the averaged migration plots.

E. Implementing the reformulated double-difference algorithm for a vertical array

The modeled RTOA and RDEA differences in the right-hand sides of Eqs. (9) and (10) were computed using the ray-tracing program BELLHOP (Porter and Reiss, 1984; Porter, 1991). Eigenrays were computed using a fan of 3000 rays from −16 to 16 degrees, and a step size of 10 m, yielding an estimated "miss" criteria of ∼10 m for logging an eigenray. Each modeled ray is then matched with a particular measured ray, based on the smallest difference in elevation angle between the model and measurement. If the minimum difference exceeded 1.5°, data associated with that measured ray path were discarded from the iteration.

The ray derivatives in Eq. (9) were computed analytically in terms of the ray parameter and the vertical slowness, using Eqs. (7) and (8). The ray derivatives in Eq. (10), while also having analytical solutions (see Appendix A), were instead calculated numerically from BELLHOP by modeling sources with small offsets in range and depth from a reference position and obtaining the angular shifts. Equations (9) and (10) are iterated until the value of **m** either converges or settles into an alternating cycle. In the latter case, the maximum value of **m** obtained during the cycle is used to compute the final residuals **d**.

To generate a complete trajectory, the first set of events is assigned initial modeled positions (i.e., initial guess for the absolute position) based on either ray-tracing or the known position. For subsequent events in the track, the initial modeled positions are then based on the result of the previous double-difference computation, as discussed above. Positional errors for the double-difference estimates are computed as shown in Sec. II D.

Figure 5(b) shows a typical example where rays do not converge at a single point. The algorithm used to produce ray-tracing position estimates as well as their associated errors is presented in Appendix B.

IV. RESULTS

The vertical array double-difference algorithm is first tested on the towed acoustic source by comparing the results to the measured trajectory of the source during two distinct phases of the source deployment: a horizontal source tow and a vertical haul during the source recovery. For each case, trajectories obtained from individually ray-tracing each event in the track are also shown. A comparison between the full double-difference and the RTOA-only approach is also presented for the vertical haul trajectory. Finally, the full double-difference technique is applied to a 25-min sperm whale track.

A. Towed acoustic source

1. Horizontal tow

Figures 7(a) and 7(c) display the depth and range, respectively, of the towed source over a 20 min period, when the source is being towed from 47 to 48 km range from the array, bouncing between depths of 160 and 180 m. Figures 8(a) and 8(c) plot RTOA and elevation angle measurements, respectively, from nine events, which are 2–4 min apart, where three rays were identified in each event. The angular measurements show that ray 1 increases by 1 degree over the 20 min period at a fairly constant rate, whereas rays 2 and 3 fluctuate over a 1–2 degree window and do not show a clear trend. The RTOA of rays 2 and 3 both show a fairly steady increase of 8 and 4 ms, respectively, with respect to ray 1, chosen here as the reference ray.

Figure 9 shows the corresponding double-difference results, plotted both in terms of absolute [Figs. 9(a) and 9(c)] and relative [Figs. 9(b) and 9(d)] depth and range (with the latter being defined relative to the location of the first event). Also plotted are the measured positions of the source, as well as localization estimates based on ray-tracing individual events. Vertical bars show the uncertainties associated with each technique. The initial modeled positions for the first pair of events were set to 46.8 km in range and 150 m in depth. Figures 9(b) and 9(d) illustrate how the ray-tracing results diverge from the measured range of the source, while also yielding larger uncertainties for both range (±100–500 m) and depth (±10–40 m), as seen in Figs. 9(b) and 9(d). By

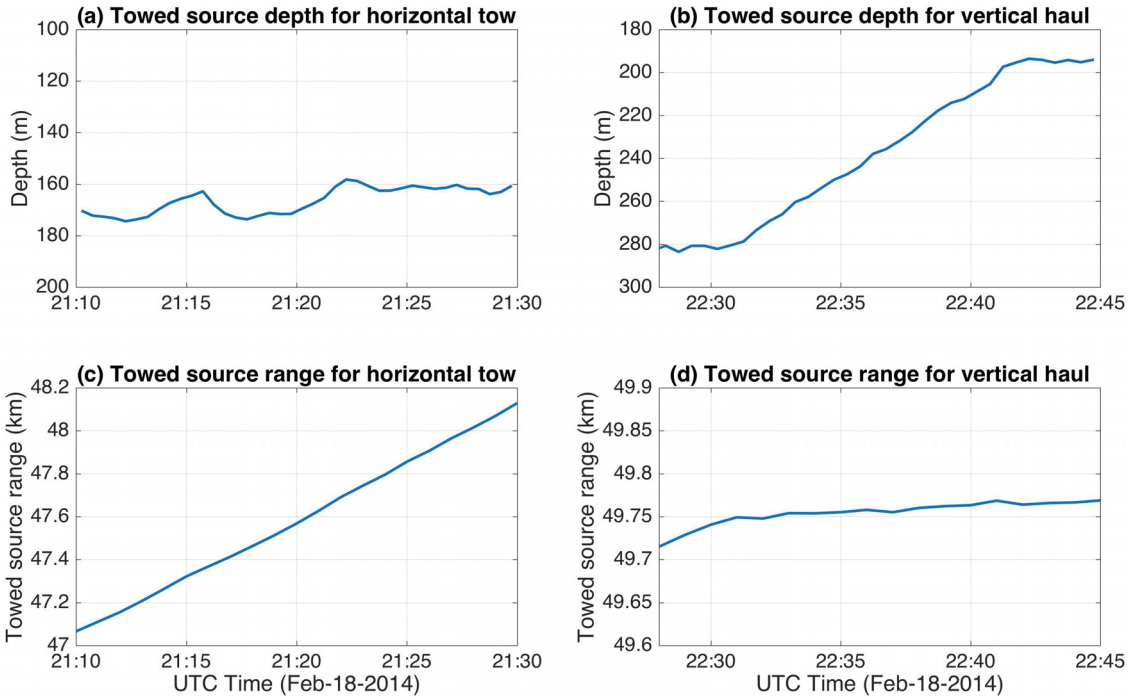

FIG. 7. (Color online) Depth and range trajectories of the acoustic source for the horizontal tow from to 21:10 to 21:30 UTC (a),(c), and the vertical haul from 22:30 to 22:45 UTC (b),(d), on February 18, 2014.

contrast, the double-difference method accurately reconstructs the relative trajectory of the source within a few meters of the measured depth trajectory and less than 100 m for the range trajectory, with uncertainties approximately an order of magnitude smaller than for the ray-tracing.

2. Vertical haul

Over this 20 min period the vessel was stationary at around 49.75 km range, while hauling the source back toward the surface, from 280 to 200 m depth. Figures 7(b) and 7(d) show the depth and range trajectories, respectively, of the source between 22:28 and 22:40 UTC. Over that same period, Figs. 8(b) and 8(d) show the RTOA and elevation angles, respectively, measured from seven events, spaced in 2 min intervals. Four to five rays were identified for each event. The elevation angles of all the rays remain fairly steady over this time period, but the RTOA of rays 2 to 5 (relative to ray 1) begin decreasing at a fairly constant rate around 22:32 UTC, which is when the source begins its vertical ascent. The decrease of RTOA spans from about 5 ms to almost 20 ms depending on the ray.

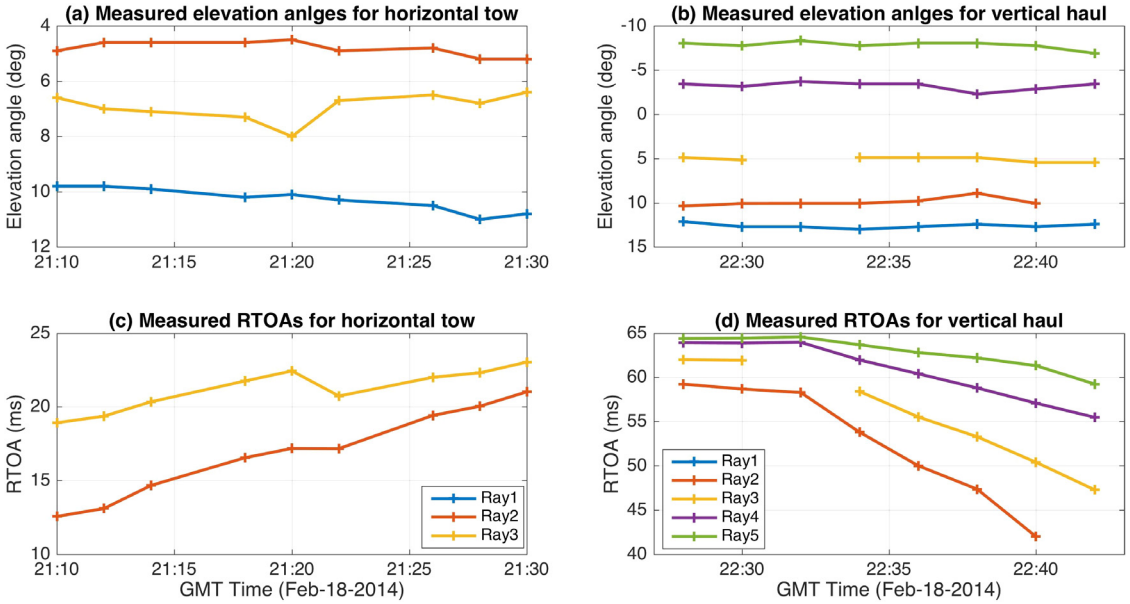

FIG. 8. (Color online) Elevation angle and RTOA measurements from the acoustic source signals for the horizontal tow from to 21:10 to 21:30 UTC (a),(c), and the vertical haul from 22:28 to 22:40 UTC (b),(d), on February 18, 2014.

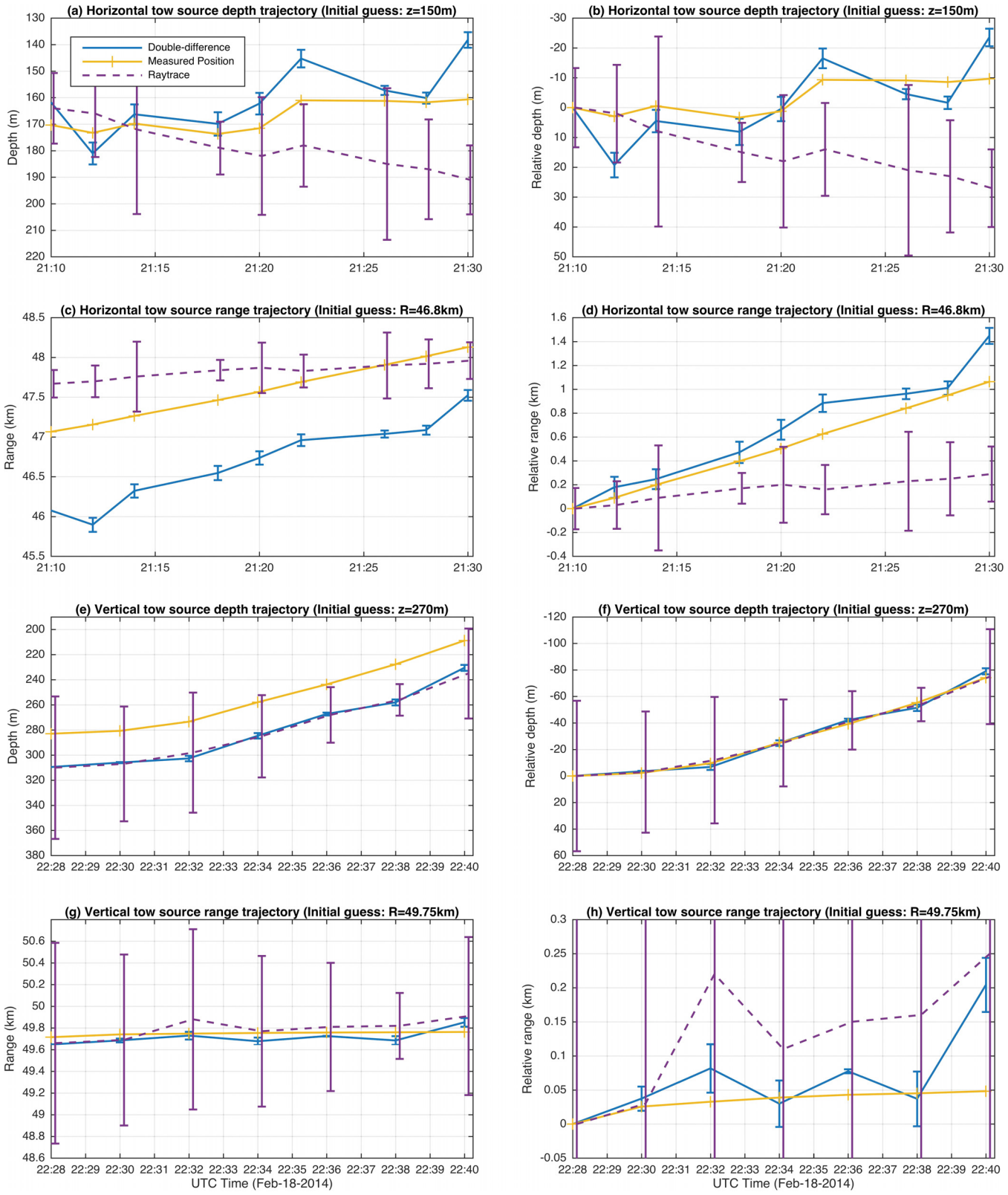

FIG. 9. (Color online) Depth and range trajectories of the towed acoustic source: double-difference results, ray-tracing results, and measured position. The top four plots show the horizontal tow and the bottom four plots show the vertical haul. The left and right columns show the trajectories in term of the absolute and relative positions, respectively. Note that the vertical scale of (h) is different than the vertical scale of (g).

Figures 9(e)–9(h) show the measured, ray-traced, and double-difference position estimates for each event, in terms of both absolute [Figs. 9(e) and 9(g)] and relative [Figs. 9(f) and 9(h)] depth and range. The initial modeled positions for the first pair of events were set to 49.75 km in range and 270 m in depth. Figure 9(f) shows that both the double-difference and the ray-tracing produce accurate depth trajectories, within a few meters of the measured position, but

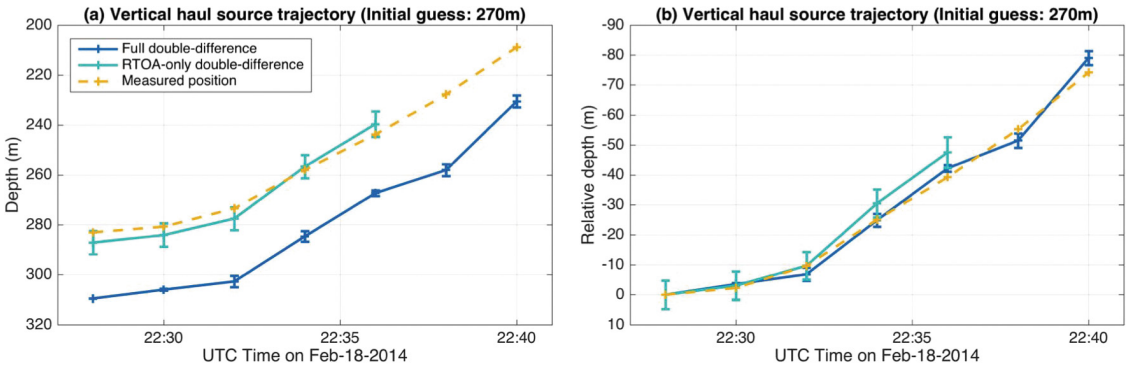

FIG. 10. (Color online) Absolute (a) and relative (b) depth trajectories of the towed acoustic source: "full" double-difference results, "RTOA-only" double-difference results, and measured depth.

Fig. 9(h) shows that ray-tracing is less accurate at reproducing the range trajectory, with biases on the order of 200 m, versus the 100 m for the double-difference. Even more striking are the relative uncertainties in position estimates between the two methods: ray-tracing produces uncertainties on the order of tens of meters in depth and hundreds of meters in range [Fig. 9(g)], in comparison with the uncertainty in depth and range [Fig. 9(h)] for the double difference results, which are an order of magnitude smaller.

Figure 10 compares the full double-difference results for the depth trajectory of the vertical haul with an RTOA-only double-difference computation. This particular scenario was selected for this comparison because it was one of the few situations where sufficient ray paths existed per event to provide a solution in terms of RTOA only. The results show that the RTOA-only double-difference performs very similarly to the full double-difference approach, but fails to converge for the last few events of the trajectory, yielding an incomplete track. The uncertainties of the RTOA-only approach are also greater than the full solution.

B. Sperm whale track

RTOA and elevation angle measurements were taken from 15 sperm whale click events over a 25 min period at intervals of 1, 2, and 4 min. During its dive the whale's inter-click interval (average time between clicks in a series of clicks) stayed nearly constant at around 0.7 s. Figure 11 indicates three consistent ray paths were identified throughout the track. The angular measurements show that ray 1 increases by about 1 degree at a relatively steady rate, whereas rays 2 and 3 remain fairly constant. RTOA measurements of these rays show a clear overall increase of about 15–20 ms (relative to ray 1) throughout the track.

The true position of the animal is unknown in this case, but results from applying the double-difference method can still be compared to ray-tracing estimates from the individual events in this track. The initial modeled positions for the first pair of events were set to 46 km in range and 350 m in depth, based on initial ray-tracing estimates.

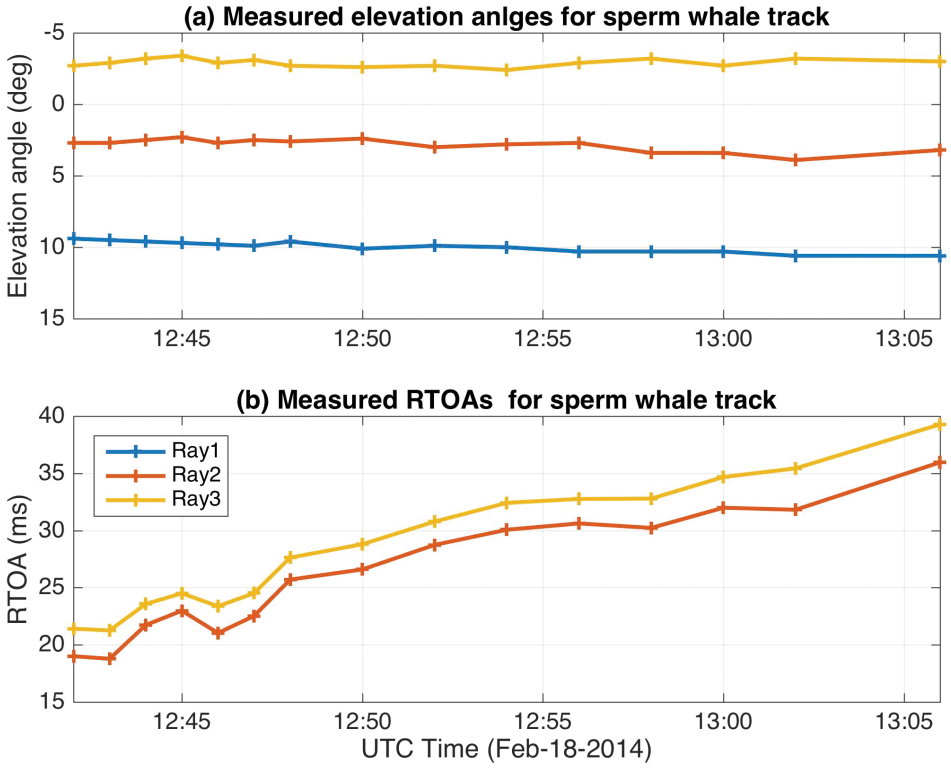

FIG. 11. (a) (Color online) Elevation angle and (b) RTOA measurements from the sperm whale track between 12:42 and 13:06 UTC on February 18, 2014.

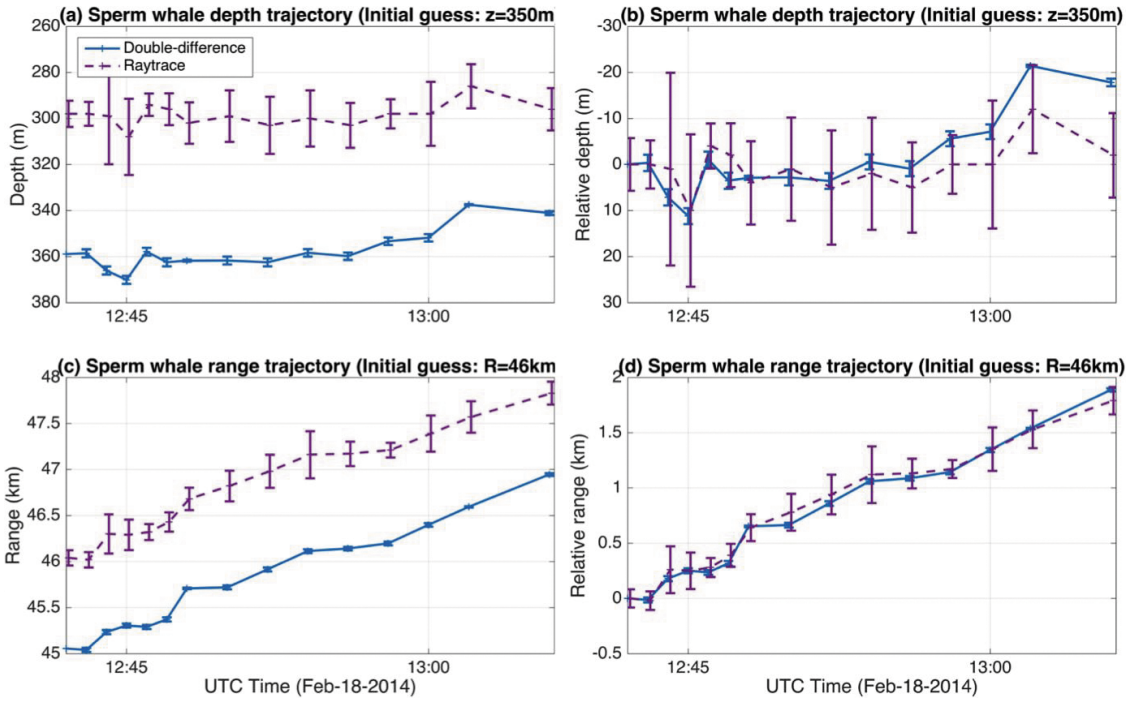

FIG. 12. (Color online) Sperm whale track between 12:42 and 13:06 UTC on February 18, 2014: double-difference results and ray-tracing results. The left and right columns show the trajectories in term of the absolute and relative positions, respectively.

The resulting trajectories (Fig. 12) show that the sperm whale remains at a fairly constant depth, between approximately 360 and 380 m, and travels from 45 to 47 km away from the vertical array. The double-difference and ray-tracing produce similar trajectories, but once again the double-difference approach yields relative uncertainties that are almost negligible (6–22 m in range and 1 m in depth) compared to ray-tracing uncertainties that are around 80–250 m in range and 5–20 m in depth.

Since the azimuth of the whale cannot be measured on the vertical array, the exact speed and heading of the whale cannot be calculated. However, a minimum and maximum possible speed can be estimated based on the geometry of the problem and assuming constant velocity. The minimum speed assumes zero heading, i.e., the animal is swimming directly away from the array, whereas the maximum speed assumes of heading of 90 degrees, with the whale swimming tangentially to the array from 45 to 47 km. Taking into account the 90 m drift of the array during time period, the possible speed of the whale ranges from 2.4 to 17.9 knots.

V. DISCUSSION

Applying the reformulated double-difference algorithm to data gathered from a field experiment shows how depth and range trajectories of both a towed acoustic source and a sperm whale can be reconstructed. This approach yields trajectories that are sometimes slightly offset from the absolute position of the source, but accurately reproduces the positions of acoustic events relative to each other (relative trajectory), as seen throughout Fig. 9. These double-difference trajectories are also shown to be more precise than those obtained using standard ray-tracing, with localization uncertainties an order of magnitude smaller than the ray-tracing uncertainties. The improved performance of the double-difference versus ray-tracing was particularly obvious for the range estimates of the controlled acoustic source, as seen in Figs. 9(d) and 9(h).

Both the full and RTOA-only double-difference methods were tested on the same data (see Fig. 10). The outcome of this analysis demonstrates that both approaches perform similarly, as long as there are enough matching rays between the model and the measurements for a given pair of events. This requires not only that the ray structure between two events be similar, but also that these rays be identified and measured in the data. If this requirement is not met, the double-difference equations become under-determined. This can be observed in Fig. 10, which shows an incomplete track for the RTOA-only double-difference that resulted from insufficient numbers of rays to permit a least-squares solution. Even though four to five rays were identified in this trajectory [see Figs. 8(b) and 8(d)], the results suggest only two of these rays were successfully matched with the model, which permitted solutions for the full double-difference but not for the RTOA-only approach. An advantage however, of the RTOA-only algorithm is that it does not need to repeatedly run BELLHOP to compute the angular derivatives in Eq. (11), making it less computationally expensive. The RTOA-only double-difference can therefore be a more efficient approach as long as, for each iteration, there are at least three matching rays between the model and the measurements of a given event pair. This is sometimes a challenging requirement, so the full double-difference approach, which requires only two matching rays and also produces smaller errors, is generally considered more robust.

The importance of matching ray arrivals between the model and the data is also clear whenever testing the robustness of the double-difference method to uncertainties in array

tilt and perturbations in the sound speed profile. As long as sufficient rays are matched, the double-difference appears to be fairly robust to uncertainties in array tilt and sound speed. However, small perturbations can sometimes cause the modeled ray structure to change substantially, reducing the number of matching rays between events and making the system under-determined. Another key factor that can have a major impact on the results is the initial modeled position of the source. Small changes (sometimes on the order of a few meters for the depth) in the initial modeled position can cause the ray structure to change enough for the double-difference to produce an incomplete track. For each track shown here, a series of trial initial event locations was tested to determine the positions that generated enough matching ray paths across the entire sequence of events.

These analyses, including the sensitivity to initial position, suggest that the depth-dependent sound speed profile variability is an important factor when considering the robustness of the approach. Indeed, the depths analyzed here are all below 400 m, a region where the sound speed changes rapidly with depth, as seen in Fig. 5. The ray structure can therefore vary rapidly with depth in this shallow region, which would explain why the double-difference results are sometimes sensitive to small changes in initial modeled position and other perturbations such as array tilt and sound speed. If true, this hypothesis predicts that double-difference approaches could be even more robust for deeper sources in the water column, where the variability of the sound speed profile is smaller. This depth-dependent environmental variability might also explain the similarity in performance between the double-difference and the ray-tracing results for the vertical haul, as seen in Figs. 9(b) and 9(f).

The double-difference was implemented here assuming a locally "homogenous" environment [Eqs. (9) and (10)], which permitted the separations between any given pair of events to be solved separately from all other events in a trajectory. Attempts to implement the "inhomogeneous" version of the problem [Eqs. (4) and (5)], where the relative positions of all events in a trajectory are computed simultaneously in one single matrix inversion (WE), were unsuccessful because it was challenging to discover initial modeled positions that yielded the required number of matching rays throughout the entire sequence of events. Had we made RTOA or RDEA measurements between all possible combinations of events, and not just events adjacent in time, we might have made more progress with the inhomogeneous formation. However, Fig. 9 shows that the homogenous formulation of the double-difference equations produced satisfying results, showing that shifts in source position on the order of a few meters could be measured accurately at ranges of nearly 50 km, even in a portion of the water column with a strong sound speed gradient.

Results also show that this method could track a sperm whale over 25 min, as seen in Fig. 12. The double-difference analysis reveals that the animal is holding a fairly steady depth within 10 m of its original position, while steadily increasing its range. Observations this precise would have been impossible with the high-uncertainty trajectory measurements resulting from standard ray-tracing. The estimated speed window of 2.4–17.9 knots spans known sperm whale swimming speeds found in the literature (Miller *et al.*, 2004; Aoki *et al.*, 2007).

VI. CONCLUSION

The double-difference method, initially developed to localize earthquakes by WE and recently applied to fin whales (Wilcock, 2012), has been reformulated here for localizing sources using multipath arrival information (RDEA and RTOA) detected on an array of sensors. This reformulation has been applied for long-range tracking of moving acoustic sources on an array whose aperture is short relative to the water depth.

Results show that relative depth and range trajectories of a towed acoustic source, located about 50 km from the array, can be accurately recovered using this method. Comparing these results to a standard ray-tracing algorithm found that the double-difference method yielded more accurate range trajectories of moving sources, and produced range and depth error estimates at least an order of magnitude smaller than ray-tracing approaches, even those that incorporated least-square fits of RTOA data. This method was also used to track the movements of a sperm whale over a 25 min period, yielding information on an animal's swimming and diving behavior.

At least two common ray paths must be identified between the model and the measurements for pairs of events, which can be challenging in an environment in which the sound speed changes rapidly with depth, but becomes feasible as more events become available to process, permitting RTOA and RDEA measurements from more combinations of events.

ACKNOWLEDGMENTS

We would like to thank William Wilcock, Peter Shearer, and John Hildebrand for their comments on this work, as well as David Ensberg, who provided useful information related to the data and the experiment. We also thank the crew of the R/V Melville, who assisted in the deployment of the array and acoustic source. The MFNA experiment was sponsored by the Office of Naval Research. This work was also partially supported by Grant No. N000141410403 from the Office of Naval Research Marine Mammal Program.

APPENDIX A: RAY DERIVATIVES FOR ELEVATION ANGLE

The analytical forms of the derivatives in Eqs. (5) and (10) are given by

$$\frac{d\theta}{dR} = \frac{1}{\eta(z_r)}\left(\frac{d^2\tau}{dp^2}\right)^{-1}, \tag{A1}$$

$$\frac{d\theta}{dz} = \frac{p}{\eta(z_s)\eta(z_r)\left(\frac{d^2\tau}{dp^2}\right)^{-1}}, \tag{A2}$$

where τ is known as the delay time, p is the ray parameters, η is the vertical slowness, and z_r and z_s are the receiver and source depths, respectively (Frisk, 1994; Shearer, 1999). In

practice, the evaluation of these derivatives is vulnerable to numerical instabilities, so for practical applications these derivatives were simply numerically evaluated by perturbing BELLHOP runs, as explained in Sec. III E.

APPENDIX B: RAY-TRACING LOCALIZATION ALGORITHM

Acoustic events were localized based on a least-squares approach, which was equivalent to a maximum-likelihood approach for this dataset. For each individual event, measured elevation angles were first propagated back into the waveguide from the array using BELLHOP. A rectangular region was then selected around the most likely convergence zone and the eigenrays were computed for each point in the grid (depth interval: 1 m, range interval: 10 m). For each grid point that produced enough rays to be matched with the measurements, the log-likelihood function was computed based on the following expression:

$$L = -\frac{1}{2\sigma_\theta^2}\sum_{i=1}^{N}\left(\theta_i^{\text{meas}} - \theta_i^{\text{mod}}\right)^2 - \frac{1}{2\sigma_T^2}\sum_{i=1}^{N}\left(\left(T_i^{\text{meas}} - T_0^{\text{meas}}\right) - \left(T_i^{\text{mod}} - T_0^{\text{mod}}\right)\right)^2, \tag{B1}$$

where θ_i and T_i are the elevation angle and travel time of the ith ray, T_0 is the travel time of the reference ray, σ_θ^2 and σ_T^2 are the estimated variances in the measured elevation angles and travel times, respectively, using the migration plots shown in Fig. 6. The depth and range of the event was then determined by locating the minimum of the log-likelihood over the search grid.

The error was then computed by running the localization algorithm 50 times with random perturbations in both the elevation angle and RTOA measurements, following a normal distribution with variances σ_θ^2 and $2\sigma_T^2$, respectively. The error bars for the ray-tracing displayed in Figs. 9 and 12 are the standard deviations of the localization results from these 50 iterations.

[1]See supplementary material at https:doi.org/10.1121/1.5014050 for a diagram of the MFNA deployment configuration.

Aoki, K., Amano, M., Sugiyama, N., Muramoto, H., Suzuki, M., Yoshioka, M., Mori, K., Tokuda, D., Miyazaki, N., and IEEE (**2007**). "Measurement of swimming speed in sperm whales," in *2007 Symposium on Underwater Technology and Workshop on Scientific Use of Submarine Cables and Related Technologies*, Vols. 1 and 2, pp. 467–471.

Cornuelle, B. D. (**1985**). "Simulations of acoustic tomography array performance with untracked or drifting sources and receivers," J. Geophys. Res.: Oceans **90**, 9079–9088, https://doi.org/10.1029/JC090iC05p09079.

Evensen, G. (**2009**). *Data Assimilation: The Ensemble Kalman Filter*, 2nd ed. (Springer, Berlin), pp. 1–307.

Fizell, R. G., and Wales, S. C. (**1985**). "Source localization in range and depth in an Arctic environment," J. Acoust. Soc. Am. **78**, S57–S58.

Fremont, M. J., and Malone, S. D. (**1987**). "High-precision relative locations of earthquakes at mount St. Helens, Washington," J. Geophys. Res., [Solid Earth Planets] **92**, 10223–10236, https://doi.org/10.1029/JB092iB10p10223.

Frisk, G. V. (**1994**). *Ocean and Seabed Acoustics: A Theory of Wave Propagation* (Prentice Hall, Englewood Cliffs, NJ), pp. 1–300.

Goold, J. C., and Jones, S. E. (**1995**). "Time and frequency-domain characteristics of sperm whale clicks," J. Acoust. Soc. Am. **98**, 1279–1291.

Ito, A. (**1985**). "High-resolution relative hypocenters of similar earthquakes by cross-spectral analysis method," J. Phys. Earth **33**, 279–294.

Locarnini, R. A., Mishonov, A. V., Antonov, J. I., Boyer, T. P., Garcia, H. E., Baranova, O. K., Zweng, M. M., Paver, C. R., Reagan, J. R., Johnson, D. R., Hamilton, M., Seidov, D., and Levitus, S. (**2013**). *World Ocean Atlas 2013, Volume 1, Temperature* (National Oceanographic Data Center, Ocean Climate Laboratory, and United States National Environmental Satellite Data and Information Service, Silver Spring, MD), pp. 1–40.

Mathias, D., Thode, A. M., Straley, J., and Andrews, R. D. (**2013**). "Acoustic tracking of sperm whales in the Gulf of Alaska using a two-element vertical array and tags," J. Acoust. Soc. Am. **134**, 2446–2461.

Miller, P. J. O., Johnson, M. P., Tyack, P. L., and Terray, E. A. (**2004**). "Swimming gaits, passive drag and buoyancy of diving sperm whales *Physeter macrocephalus*," J. Exp. Biol. **207**, 1953–1967.

Porter, M., and Reiss, E. L. (**1984**). "A numerical-method for ocean-acoustic normal-modes," J. Acoust. Soc. Am. **76**, 244–252.

Porter, M. B. (**1991**). "The KRAKEN normal mode program," SACLANT Undersea Research Centre, La Spezia, Italy.

Poupinet, G., Ellsworth, W. L., and Frechet, J. (**1984**). "Monitoring velocity variations in the crust using earthquake doublets—An application to the Calaveras fault, California," J. Geophys. Res. **89**, 5719–5731, https://doi.org/10.1029/JB089iB07p05719.

Press, W. H. (**1992**). *Numerical Recipes in FORTRAN: The Art of Scientific Computing* (Cambridge University Press, Cambridge, UK), pp. 1–973.

Shearer, P. M. (**1997**). "Improving local earthquake locations using the L1 norm and waveform cross correlation: Application to the Whittier Narrows, California, aftershock sequence," J. Geophys. Res.: Solid Earth **102**, 8269–8283, https://doi.org/10.1029/96JB03228.

Shearer, P. M. (**1999**). *Introduction to Seismology* (Cambridge University Press, Cambridge, NY), pp. 1–396.

Skolnik, M. I. (**1962**). *Introduction to Radar Systems* (McGraw-Hill, New York), pp. 1–581.

Thode, A. (**2004**). "Tracking sperm whale (*Physeter macrocephalus*) dive profiles using a towed passive acoustic array," J. Acoust. Soc. Am. **116**, 245–253.

Thode, A., Mellinger, D. K., Stienessen, S., Martinez, A., and Mullin, K. (**2002**). "Depth-dependent acoustic features of diving sperm whales (*Physeter macrocephalus*) in the Gulf of Mexico," J. Acoust. Soc. Am. **112**, 308–321.

Tiemann, C. O., Thode, A. M., Straley, J., O'Connell, V., and Folkert, K. (**2006**). "Three-dimensional localization of sperm whales using a single hydrophone," J. Acoust. Soc. Am. **120**, 2355–2365.

Waldhauser, F., and Ellsworth, W. L. (**2000**). "A double-difference earthquake location algorithm: Method and application to the northern Hayward fault, California," Bull. Seismolog. Soc. Am. **90**, 1353–1368.

Watkins, W. A., and Schevill, W. E. (**1972**). "Sound source location by arrival-times on a non-rigid three-dimensional hydrophone array," Deep-Sea Res. **19**, 691–706.

Wilcock, W. (**2012**). "Tracking fin whales in the northeast Pacific Ocean with a seafloor seismic network," J. Acoust. Soc. Am. **132**, 2408–2419.

Zimmer, W. M. X., Johnson, M. P., D'Amico, A., and Tyack, P. L. (**2003**). "Combining data from a multisensor tag and passive sonar to determine the diving behavior of a sperm whale (*Physeter macrocephalus*)," IEEE J. Ocean. Eng. **28**, 13–28.